Reduction in operating voltage of AlGaN homojunction tunnel junction deep-UV light-emitting diodes by controlling impurity concentrations

Kengo Nagata[1,2,3*], Hiroaki Makino[2], Hiroshi Miwa[2,3], Shinichi Matsui[2,3], Shinya Boyama[2,3], Yoshiki Saito[2,3], Maki Kushimoto[1], Yoshio Honda[4], Tetsuya Takeuchi[5], and Hiroshi Amano[4]

[1]*Graduate School of Engineering, Nagoya University, Furo-cho, Chikusa-ku, Aichi 464-8603, Japan*

[2]*Toyoda Gosei Co., Ltd., 710 Shimomiyakeoriguchi, Heiwa-cho, Inazawa, Aichi, 290-1312, Japan*

[3]*TS Opto Co., Ltd., 5-1, Yawatakaigandori, Ichihara, 290-0067, Chiba, Japan*

[4]*Center for Integrated Research of Future Electronics, Institute of Materials Research and System for Sustainability, Nagoya University, Furo-cho, Chikusa-ku, Aichi 464-8601, Japan*

[5]*Faculty of Science and Technology, Meijo University, 1-501 Shiogamaguchi, Tenpaku-ku, Aichi 468-8502, Japan*

[*]E-mail: nagata.kengo@c.mbox.nagoya-u.ac.jp, kengo.nagata@toyoda-gosei.co.jp

We reduced the operating voltage of AlGaN homojunction tunnel junction (TJ) deep-ultraviolet (UV) light-emitting diodes (LEDs) by two approaches: the suppression of carbon incorporation and the doping of a high concentration of silicon in an n^+-AlGaN layer. The AlGaN homojunction TJ deep-UV LEDs had a significantly reduced forward voltage upon suppressing the incorporation of carbon in the n^+-AlGaN layer The suppression of electron compensation by carbon in nitrogen sites and the doping of a high concentration of silicon in an n^+-AlGaN layer are important for reducing the operating voltage of AlGaN homojunction TJ deep-UV LEDs.

Aluminum gallium nitride (AlGaN)-based light-emitting devices (LEDs) can realize deep-ultraviolet (UV) emission from the UV-A region (365 nm) to the UV-C region (210 nm). Instead of conventional mercury lamps, deep-UV LEDs are promising for a wide range of applications such as sterilization, purification, bio/chemical sensing, resin curing, and medical treatment. Recently, some research groups reported the room-temperature pulsed laser oscillation of deep-UV laser diodes, 1, 2) demonstrating the high potential of AlGaN for UV emitters. On the other hand, recent reports indicate that external quantum efficiencies (EQEs) of more than 10% were achieved for deep-UV LEDs, with emission wavelengths of approximately 280 nm.3–8) However, further improvements in EQE are required for high-power applications because it is necessary to make a module equipped with multiple LED chips, marking the manufacturing cost extremely high. Additionally, an improvement in wall-plug efficiency (WPE) is also desired to replace mercury lamps. The WPE is expressed by the product of three efficiencies: internal quantum efficiency (IQE), light extraction efficiency (LEE), and driving efficiency (DE) including joule loss and current injection loss. Of these efficiencies, the LEE of deep-UV LEDs is extremely low, which is mainly caused by the absorption of the top p-type gallium nitride (p-GaN) in the device layer structure. The light emitted from the quantum well layer to the p-GaN side is fully absorbed. On the other hand, the light to the n-layer side is mostly reflected at the interface between air and sapphire or aluminum nitride (AlN), and is mostly absorbed by the p-GaN layer. To improve the LEE of deep-UV LEDs, it is necessary to have a structure without GaN such as a p-AlGaN contact or AlGaN-based tunnel junction (TJ) structures. Some research groups have reported a high LEE in a p-AlGaN contact structure with high reflective electrodes such as Ni/Al and Rh, 4, 9–11) which achieved a high output power and a low operating voltage. However, no ohmic contact has been obtained with the Al composition of 50% or more in the p AlGaN contact layer. On the other hand, in some reports, the reported AlGaN-based TJ deep-UV LEDs have realized device operation at a low voltage with the insertion of an interlayer such as GaN or gallium indium nitride between the TJ layers, in which polarization-assisted tunneling was used. 12-14) However, there is serious light absorption in the thin interlayer owing to a lower bandgap energy than in AlGaN multi-quantum wells (MQWs). Higher output power deep-UV LEDs need high-Al-composition AlGaN-based TJs without such a lower bandgap interlayer. Some research groups reported AlGaN homojunction TJ deep-UV LEDs, that operated at high voltages of 13 – 50 V.[13, 15, 16] The operating voltage is still very high. Therefore, it is necessary to increase the tunnel probability of the TJ layer by reducing the depletion region. In principle, a TJ uses a quantum tunneling phenomenon, [17, 18] in which electrons transit from the valence band to the conduction band. To induce the transition, the impurity needs to be highly doped, in other words, degenerate semiconductors in both n-AlGaN and p-AlGaN are necessary. Here, the effective densities of states in the conduction and valence bands for $Al_{0.6}Ga_{0.4}N$ are estimated to be 4.5×10^{18} cm^{-3} and 2.4×10^{20} cm^{-3} at room temperature (RT), respectively. [19, 20] However, III-nitride semiconductors suffer from a low tunneling probability owing to the difficulty in achieving degenerate impurity doping and a high potential barrier. It is more difficult to change the higher activation energies of impurities, such as magnesium (Mg) and silicon (Si), and the higher potential barrier as the Al composition increases. We have reported the low resistivity and electronic degeneracy conduction in n-$Al_{0.6}Ga_{0.4}N$.[21, 22] We have confirmed that the $N_D - N_A$ value of 9.5×10^{18} cm^{-3} nullifies the ionization energy of Si donors, which is almost six times higher than that in GaN.[21] However, the n-$Al_{0.6}Ga_{0.4}N$ layer with an overdoped Si concentration (> 6×10^{19} cm^{-3}) has an extremely high resistivity and does not degenerate owing to self-compensation by cation-vacancy–silicon (V_{III}-nSi) complexes,[21−27] In addition, carbon atoms possibly cause electron compensation because they occupy carbon on nitrogen sites (C_N), which is the same effect as in n-GaN.[21, 22, 28, 29] In this work, we demonstrate transparent AlGaN homojunction TJ deep-UV LEDs with Al compositions of more than 50% by controlling the growth pressure to suppress carbon incorporation. We also evaluate the characteristics of the TJ deep-UV LEDs with high Si concentrations in the TJ layers for a high tunneling probability.

The deep-UV LED structures were grown by low-pressure MOVPE on 4-inch flat (0001) sapphire substrates with a miscut angle of 0.35° toward the sapphire $[11\bar{2}0]$ direction. Trimethylaluminium (TMAl), trimethylgallium (TMGa), triethylgallium (TEGa), and ammonia (NH_3) gases as Al, Ga, and N sources, respectively, were supplied to a reactor using hydrogen (H_2) carrier gas. Bis(cyclopentadienyl)magnesium and monosilane (SiH_4) gas were used as Mg and Si sources, respectively. After the thermal cleaning of the sapphire substrates in H_2 atmosphere to reduce the threading dislocation density, the AlN template layer was grown by a two-step growth process of nucleation at a surface temperature of

1100 °C and the subsequent flattering growth of a 3-μm-thick layer at a surface temperature of 1270 °C.30, 31) The threading dislocation densities of screw and edge dislocations including mixed components in the AlN-template estimated from the X-ray rocking curve were 9 × 10^7 cm^{-2} and 1 × 10^9 cm^{-2}, respectively. 32) No pits were observed on the AlN-template surface. The 1.3 μm-thick n-type $Al_{0.62}Ga_{0.38}N$ underlayer doped with a Si concentration of 3 × 10^{19} cm^{-3} was grown on the templates.21, 22) The dislocation densities of screw and edge components in the n-type AlGaN layer were estimated to be 1 × 10^8 cm^{-2} and 9 × 10^8 cm^{-2}, respectively. The growth of the n-type AlGaN underlayer was followed by a second-period, multiple-quantum-well layer consisting of 11-nm-thick $Al_{0.55}Ga_{0.45}N$ barriers, 2-nm-thick $Al_{0.45}Ga_{0.55}N$, and an $Al_{0.85}Ga_{0.15}N$ electron blocking layer (EBL). Subsequently, two structures were grown on the AlGaN EBL, as shown in Fig. 1 and Table 1. The PN LEDs PN#1 and PN#2 consisted of 50-nm-thick p-AlGaN with Al compositions of 50% and 60% and a 20-nm-thick p^+-GaN contact layer, respectively. On the other hand, the TJ LEDs from TJ#1 to TJ#5 consisted of 50-nm-thick p-AlGaN, 50-nm-thick p^+-AlGaN, 40-nm-thick n^+-$Al_{0.6}Ga_{0.4}N$, and 270-nm-thick n-$Al_{0.6}Ga_{0.4}N$ contact layer, where the Al composition of p-AlGaN/p^+-AlGaN layers consisted of 50% from TJ#1 to TJ#4 and 60% to TJ#5, respectively. Okumura *et al.* reported that $N_A - N_D$ and activation energy in p-GaN were 7.0 × 10^{19} cm^{-3} and 29 meV, respectively.33) Kozodoy *et al.* reported that acceptor concentration and activation energy in p^+-GaN were 1.6 × 10^{20} cm^{-3} and 112 meV at a Mg concentration of 2.0 × 10^{20} cm^{-3}, respectively.34) Hence, we adopted Mg concentrations of 5.0 × 10^{19} cm^{-3} and 1.7 × 10^{20} cm^{-3} in p-AlGaN and p^+-AlGaN, respectively. We prepared the TJ LED samples from TJ#1 to TJ#5 with various impurity concentrations in n^+-AlGaN/n-AlGaN layers, as shown in Table 1. The carbon concentrations of n^+-AlGaN were approximately 3.0 × 10^{18} cm^{-3} in TJ#1 and TJ#2 and 6.5 × 10^{17} cm^{-3} in TJ#3 to TJ#5, which were controlled by growth at 50 mbar and 100 mbar, respectively. The mesa was formed by dry-etching with HCl gas. Then, we formed a V/Al/Ti/Pt/Au (20/150/50/100/240 nm) electrode for the n-AlGaN contact and an indium zinc oxide (IZO) (200 nm) electrode for the p-GaN contact for structure (a), which were annealed separately at 720°C and 350°C, respectively. We also formed V/Al/Ti/Pt/Au (20/150/50/100/240 nm) electrodes for both n-AlGaN contacts for structure (b); they were annealed simultaneously at 720°C for 30 s in nitrogen ambient. Then, the temperature was slowly lowered to 500°C over 20 min. Mg activation annealing was performed simultaneously with n-electrode annealing, where hydrogen diffused laterally through the exposed portions of p-AlGaN and p-GaN.34) The sizes of the LEDs, and anodes, and the thickness of sapphire were 1 mm^2, 0.56 mm^2, and 200 μm, respectively. The light output values were directly measured using an integrating sphere. To examine the spread of light emission in the AlGaN homojunction TJ deep-UV LED, we took a UV light-emission image obtained by using an ARTCAM-407UV-WOM CCD camera manufactured by ARTRAY.

Figure 2 shows forward voltage – current density characteristics measured by direct current (DC) operation at RT for samples PN#1, TJ#1, TJ#2, TJ#3, and TJ#4. Our standard LED of sample PN#1 exhibited a forward voltage of 6.6 V at 63 A/cm^2 and almost the same characteristics as those the reported. 7, 8, 10) TJ LEDs TJ#1 and TJ#2 exhibited a very high voltage (about 16 V at 4 A/cm^2) and could not inject sufficient current, as shown in Fig. 2. However, the forward voltage of TJ#2 tended to drop slightly compared with that of TJ#1. On the other hand, the forward voltages of TJ LEDs TJ#3 and TJ#4 significantly decreased by more than 6 V than those of TJ#1 and TJ#2, which were operated at 12.1 V and 10.3 V at 63 A/cm^2, respectively. These results showed that the doping of a high Si concentration of n^+-AlGaN was effective in reducing the forward voltage by comparing TJ#1 with TJ#2 and TJ#3 with #TJ4. On the other hand, by comparing TJ#1 with TJ#3 and TJ#2 with #TJ4, it is evident that the low concentration of C incorporated markedly reduced the forward voltage. The carrier concentration and resistivity of n^+-$Al_{0.6}Ga_{0.4}N$ in TJ#2 should be very low (< 1.0 $\times 10^{16}$ cm^{-3}) and very high (> 2,000 Ωcm) at the Si concentration of 1.2 $\times 10^{20}$ cm^{-3},19) whereas those in TJ#4 are 3.5 $\times 10^{16}$ cm^{-3} and 23 Ωcm at the Si concentration of 1.2 $\times 10^{20}$ cm^{-3}, respectively. Here, the carrier concentration and resistivity were evaluated by the van der-Pauw Hall-effect measurement at RT. The operating voltage of AlGaN homojunction TJ LEDs can be reduced because the carrier concentration of n^+-$Al_{0.6}Ga_{0.4}N$ is increased by suppressing C incorporation.

We also evaluated a PN LED consisting of p-$Al_{0.6}Ga_{0.4}N$ (PN#2) and an n-$Al_{0.6}Ga_{0.4}N$/p-$Al_{0.6}Ga_{0.4}N$ TJ LED (TJ#5) to increase LEE for the deep-UV LEDs. TJ LED TJ#5 was produced under the optimized growth conditions from the growths determined from the growths of TJ#1 to TJ#4. The characteristics of PN#2 were an output power of 35.7 mW, an operating voltage of 7.2 V, and a wavelength of 285 nm at RT and 63 A/cm^2 with DC operation, as shown in Figs. 3 and 4. The operating voltage slightly increased by approximately 0.6 V as the Al composition of p-AlGaN changed from 50% to 60%. The injection current dependence of output power is linear and is not affected by current droop. The p-GaN contact layer and p contact electrode of IZO absorbed photons below 3.4 eV and about 2.9 eV, respectively. Therefore, the emitted UV light was almost completely absorbed at the p-side. On the other hand, TJ LED TJ#5 operated similarly to TJ#4 and the characteristics were an output power of 27.6 mW, an operating voltage of 10.8 V, and a wavelength of 280 nm at RT and 63 A/cm^2 with DC operation. There was an increase of 0.5 V with TJ#4. However, for TJ#5, the injection current dependence of the output power was nonlinear and slight output power droop occurred at more than 40 A/cm^2. Figure 5 shows a LED chip on a mounting board and UV light emission images of the AlGaN homojunction TJ deep-UV LED at an injection current of 3.6 A/cm^2. The UV light emission pattern maintains a high uniformity from the initial injection current. This indicates that p-layers in the TJ LEDs had been fully activated by dehydrogenation from the mesa-processed sides.[35)]

These results suggest that the reduction in TJ resistivity results from suppressing C incorporation and doping with a high concentration of Si in n$^+$-AlGaN. There is strong donor compensation effected by, for example, Ga vacancy in n-GaN and V_{III}-nSi complexes in n-AlGaN.[21, 36, 37)] Regarding C incorporation, the carrier became n-type as the C concentration decreased by 6.5 × 10^{17} cm^{-3}, and the operating voltage of the device decreased markedly. On the other hand, when the C concentration was 1.8 × 10^{18} cm^{-3}, it became semi-insulated, and the TJ could not be formed. Therefore, $N_d - N_a$ should be between 6.5 × 10^{17} cm^{-3} and 1.8 × 10^{18} cm^{-3}. One possibility is that the potential barrier at the TJ is lower. There may be a higher Fermi level in the n$^+$-AlGaN layer. Another possibility is that the tunneling probability at the TJ is higher owing to the increase in carrier concentration in the n$^+$-AlGaN layer. If the carbon concentration can be further reduced, the operating voltage of the AlGaN homojunction TJ deep-UV LED can also be further reduced. In addition, it should be emphasized that the doping of a high concentration of Si also reduces the TJ resistivity. Highly doped donors can increase the tunneling probability of AlGaN homojunction TJs. Continuously, further experiments are needed for achieving a low operating voltage and understanding tunneling conduction mechanisms in Al-rich AlGaN TJs. In addition, there was no reflectance at the p-side as the n-electrodes sintered at high temperatures fully absorbed UV light with wavelengths below 300 nm. As a future work, an improvement in output power by about 1.3 to 2.3 times can be expected on adopting highly reflective electrodes such as aluminum and rhodium.4, 7) The high-Al-composition AlGaN homojunction TJ deep-UV LED can be expected to achieve the high WPE required in various applications.

In summary, we presented the reduction in the operating voltage of the transparent Al-rich AlGaN homojunction TJ deep-UV LEDs grown by MOVPE. $Al_{0.6}Ga_{0.4}N$ homojunction TJ deep-UV LEDs attained an operating voltage of 10.8 V and a WPE of 0.7 % at 63 A/cm^2. There were two essential factors, that is, a low carbon incorporation and a high Si concentration in the n^+-AlGaN layer, are necessary for the reduction in the operating voltage of AlGaN homojunction TJ LEDs. In the near future, a high WPE of deep UV LEDs may be achieved by combining an Al-rich AlGaN homojunction TJ LED and a highly reflective electrode.

References

1) Z. Zhang, M. Kushimoto, T. Sakai, N. Sugiyama, L. J. Schowalter, C. Sasaoka, and H. Amano, Appl. Phys. Express **12**, 124003 (2019).
2) K. Sato, S. Yasue, K. Yamada, S. Tanaka, T. Omori, S. Ishizuka, S. Teramura, Y. Ogino, S. Iwayama, H. Miyake, M. Iwaya, T. Takeuchi, S. Kamiyama, and I. Akasaki, Appl. Phys. Express **13**, 031004 (2020).
3) M. Ichikawa, A. Fujioka, T. Kosugi, S. Endo, H. Sagawa, H. Tamaki, T. Mukai, M. Uomoto, and T. Shimatsu, Appl. Phys. Express **9**, 072101 (2016).
4) T. Takano, T. Mino, J. Sakai, N. Noguchi, K. Tsubaki, and H. Hirayama, Appl. Phys. Express **10**, 031002 (2017).
5) M. Shatalov, W. Sun, A. Lunev, X. Hu, A. Dobrinsky, Y. Bilenko, J. Yang, M. Shur, R. Gaska, and C. Moe, Appl. Phys. Express **5**, 082101 (2012).
6) M. Ippommatsu, A. Hirano, I. Akasaki, and H. Amano, 2013 Conf. Lasers Electro-Opt. Pac. Rim, (Opt. Soc. Am. 2013), 2013, paper MH1_3.
7) T. Inazu, S. Fukahori, C. Pernot, M. H. Kim, T. Fujita, Y. Nagasawa, A. Hirano, M. Ippommatsu, M. Iwaya, T. Takeuchi, S. Kamiyama, M. Yamaguchi, Y. Honda, H. Amano and I. Akasaki, Jpn. J. Appl. Phys. **50**, 122101 (2011).
8) Y. J. Sung, M. S. Kim, H. Kim, S. Choi, Y. H. Kim, M. H. Jung, R. J. Choi, Y. T. Moon, J. T. Oh, H. H. Jeong, and G. Y. Yeom, Optics Express **27**, 29930 (2019).
9) N. Maeda, M. Jo, and H. Hirayama, Phys. Status Solidi A **215**, 1700435 (2018).
10) S. Y. Lee, D. S. Han, Y. G. Lee, K. K. Choi, J. T. Oh, H. H. Jeong, T. Y. Seong, and H. Amano, ECS J. Solid State Sci. Technol. **9**, 065016 (2020).
11) J. Zhang, Y. Gao, L. Zhou, Y. U. Gil, and K. M. Kim, Semicond. Sci. Technol. **33**, 07LT01 (2018).
12) Y. Zhang, Z. J. Eddine, F. Akyo, S. Bajaj, J. M. Johnson, G. Calderon, A. A. Allerman, M. W. Moseley, A. M. Armstrong, J. Hwang, and S. Rajan, Appl. Phys. Lett. **112**, 071107 (2018).
13) C. Kuhn, L. Sulmoni, M. Guttmann, J. Glaab, N. Susilo, T. Wernicke, M. Weyers, and M. Kneissl, Photonics Res. **7**, B7 (2019).
14) A. Pandey, W. J. Shin, J. Gim, R. Hovden, and Z. Mi, Photonics Res. **8**, 331 (2020).
15) V. Fan Arcara, B. Damilano, G. Feuillet, S. Vézian, K. Ayadi, S. Chenot, and J.-Y. Duboz,

J. Appl. Phys. **126**, 224503 (2019).
16) E. A. Clinton, Z. Engel, E. Vadiee, J. V. Carpenter, Z. C. Holman, and W. A. Doolittle, Appl. Phys. Lett. **115**, 082104 (2019).
17) L. Esaki, Phys. Rev., **109**, 603 (1958).
18) L. Esaki, IEEE Trans. Electron Devices **ED-23**, 644 (1976).
19) M. Suzuki, T. Uenoyama, and A. Yanase, Phys. Rev. B **58**, 10064 (1998).
20) S. Schöche, P. Kühne, T. Hofmann, M. Schubert, D. Nilsson, A. K. Georgieva, E. Janzén, and V. Darakchieva, Appl. Phys. Lett. **103**, 212107 (2013).
21) K. Nagata, H. Makino, T. Yamamoto, K. Kataoka, T. Narita, and Y. Saito, Appl. Phys. Express **13**, 025504 (2020).
22) K. Kataoka, T. Narita, K. Nagata, H. Makino, and Y. Saito, Appl. Phys. Lett. **117**, 262103 (2020).
23) T. Narita, K. Tomita, S. Yamada, and T. Kachi, Appl. Phys. Express **12**, 011006 (2019).
24) S. F. Chichibu, H. Miyake, Y. Ishikawa, M. Tashiro, T. Ohtomo, K. Furusawa, K. Hazu, K. Hiramatsu, and A. Uedono, J. Appl. Phys. **113**, 213506 (2013).
25) K. B. Nam, M. L. Nakarmi, J. Y. Lin, and H. X. Jiang, Appl. Phys. Lett. **86**, 222108 (2005).
26) N. Nepal, M. L. Nakarmi, J. Y. Lin, and H. X. Jiang, Appl. Phys. Lett. **89**, 092107 (2006).
27) J. S. Harris, J. N. Baker, B. E. Gaddy, I. Bryan, Z. Bryan, K. J. Mirrielees, P. Reddy, R. Collazo, Z. Sitar, and D. L. Irving, Appl. Phys. Lett. **112**, 52101 (2018).
28) F. Kaess, S. Mita, J. Xie, P. Reddy, A. Klump, L. H. Hernandez-Balderrama, S. Washiyama, A. Franke, R. Kirste, A. Hoffmann, R. Collazo, and Z. Sitar, J. Appl. Phys. **120**, 105701 (2016).
29) A. Wolos, Z. Wilamowski, M. Piersa, W. Strupinski, B. Lucznik, I. Grzegory, and S. Porowski, Phys. Rev. B **83**, 165206 (2011).
30) M. Imura, K. Nakano, N. Fujimoto, N. Okada, K. Balakrishnan, M. Iwaya, S. Kamiyama, H. Amano, I. Akasaki, T. Noro, T. Takagi, and A. Bandoh, Jpn. J. Appl. Phys. **45**, 8639 (2006).
31) K. Nagata, H. Makino, T. Yamamoto, Y. Saito, and H. Miki, Jpn. J. Appl. Phys. **58**, SCCC29 (2019).
32) C. G. Dunn and E. F. Koch, Acta Metall. **5**, 548 (1957).
33) H. Okumura, D. Martin, M. Malinverni, and N. Grandjean, Appl. Phys. Lett. **108**, 072102

(2016).
34) P. Kozodoy, H. Xing, S. P. DenBaars, U. K. Mishra, A. Saxler, R. Perrin, S. Elhamri, and W. C. Mitchel, J. Appl. Phys. **87**, 1832 (2000).
35) Y. Kuwano, M. Kaga, T. Morita, K. Yamashita, K. Yagi, M. Iwaya, T. Takeuchi, S. Kamiyama, and I. Akasaki, Jpn. J. Appl. Phys. **52**, 08JK12 (2013).
36) S. Fritze, A. Dadgar, H. Witte, M. Bügler, A. Rohrbeck, J. Bläsing, A. Hoffmann, and A. Krost, Appl. Phys. Lett. **100**, 122104 (2012).
37) I. Bryan, Z. Bryan, S. Washiyama, P. Reddy , B. Gaddy , B. Sarkar , M. H. Breckenridge, Q. Guo, M. Bobea, J. Tweedie, S. Mita, D. Irving, R. Collazo, and Z. Sitar, Appl. Phys. Lett. **112**, 062102 (2018).

Figure Captions

Fig. 1. Deep-UV LED structures for (a) PN and (b) TJ devices.

Table 1. Summary of evaluated parameters for all samples. PN and TJ indicate the PN junction and TJ devices, respectively. Si and C concentrations in samples TJ#1, TJ#3, and TJ#4 were directly measured for the device, while Si and C concentrations in samples TJ#2 and TJ#5 were estimated from the results for TJ#1, TJ#3, and TJ#4 (labeled by *).

Fig. 2. Forward voltage – current density characteristics measured by DC operation at room temperature for samples PN#1, TJ#1, TJ#2, TJ#3, and TJ#4.

Fig. 3. Forward voltage – current density characteristics measured by DC operation at room temperature for samples PN#2 and TJ#5.

Fig. 4. Output power – current density characteristics measured by DC operation at room temperature for samples PN#2 and TJ#5.

Fig. 5. (a) LED chip on mounting board and (b) light emission images at 3.6 A/cm^2.

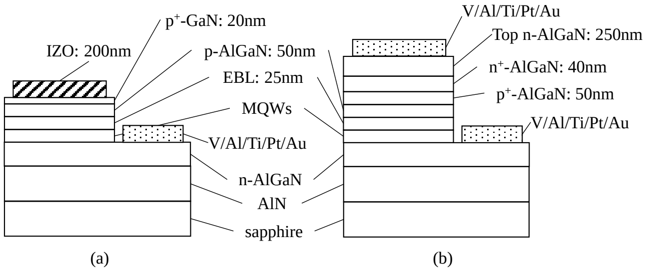

Fig.1.

(Single column)

Table 1 (double column)

Sample		p-AlGaN	p^+-AlGaN	n^+-AlGaN		Top n-AlGaN	
		Al composition		[Si] (cm^{-3})	[C] (cm^{-3})	[Si] (cm^{-3})	[C] (cm^{-3})
PN	#1	50%					
	#2	60%					
TJ	#1	50%	50%	6.2×10^{19}	1.8×10^{18}	2.2×10^{19}	3.0×10^{18}
	#2	50%	50%	1.3×10^{20}*	1.8×10^{18}*	2.2×10^{19}*	3.0×10^{18}*
	#3	50%	50%	6.3×10^{19}	6.5×10^{17}	2.6×10^{19}	3.1×10^{17}
	#4	50%	50%	1.3×10^{20}	6.5×10^{17}	2.6×10^{19}	3.1×10^{17}
	#5	60%	60%	1.3×10^{20}*	6.5×10^{17}*	2.6×10^{19}*	3.1×10^{17}*

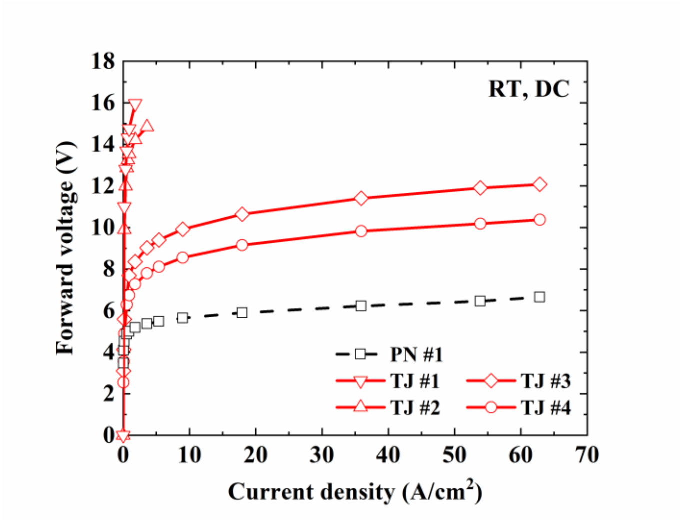

Fig. 2. (Color)

Color print

(single column)

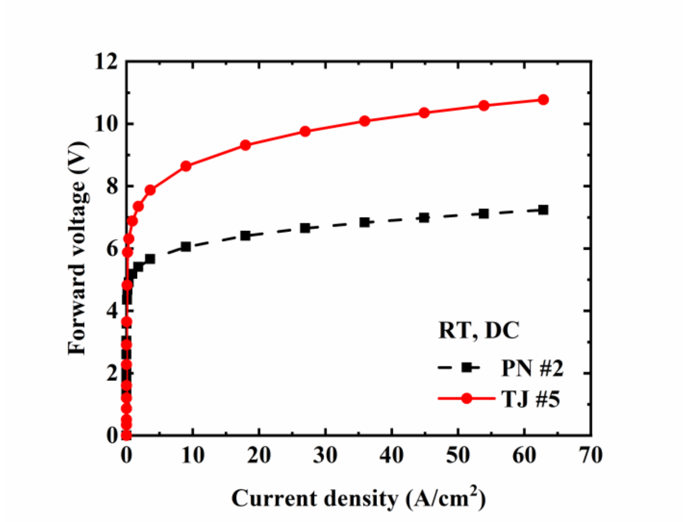

Fig. 3. (Color)

Color print

(single column)

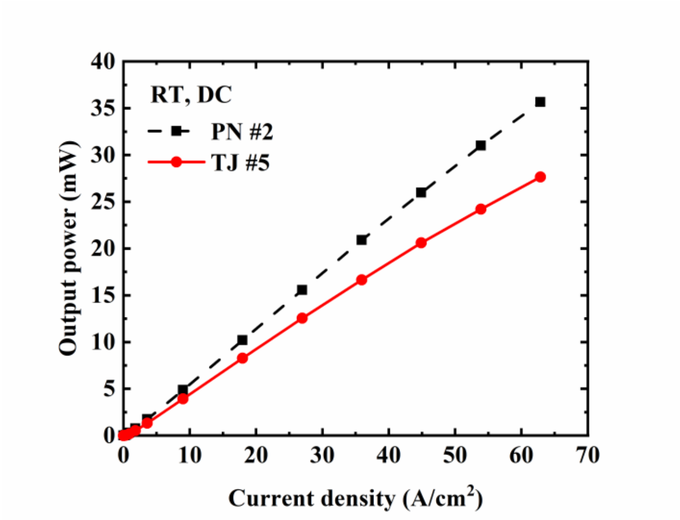

Fig. 4. (Color)

Color print

(single column)

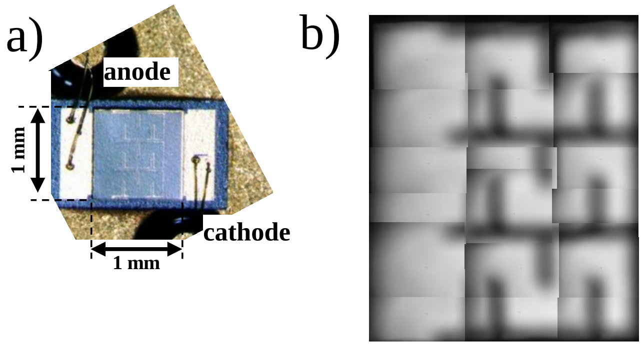

Fig. 5. (Color)

Color print

(single column)